Applied Mathematics and Computation 262 (2015) 15–30

Contents lists available at ScienceDirect

Applied Mathematics and Computation

journal homepage: www.elsevier.com/locate/amc

Central finite volume schemes on nonuniform grids and applications

R. Touma [a,*], D. Zeidan [b], S. Habre [a]

[a] Department of Computer Science and Mathematics, Lebanese American University, Beirut, Lebanon
[b] School of Basic Sciences and Humanities German Jordanian University, Amman, Jordan

ARTICLE INFO

This paper is dedicated to the memory of professor Paul Arminjon (1941–2011).

Keywords:
Central schemes
Nonuniform grids
Nonoscillatory
Unstaggered grids
Two-phase flows
Euler systems with gravity

ABSTRACT

We propose a new one-dimensional unstaggered central scheme on nonuniform grids for the numerical solution of homogeneous hyperbolic systems of conservation laws with applications in two-phase flows and in hydrodynamics with and without gravitational effect. The numerical base scheme is a generalization of the original Lax–Friedrichs scheme and an extension of the Nessyahu and Tadmor central scheme to the case of nonuniform irregular grids. The main feature that characterizes the proposed scheme is its simplicity and versatility. In fact, the developed scheme evolves a piecewise linear numerical solution defined at the cell centers of a nonuniform grid, and avoids the resolution of the Riemann problems arising at the cell interfaces, thanks to a layer of staggered cells used intermediately. Spurious oscillations are avoided using a slopes limiting procedure. The developed scheme is then validated and used to solve classical problems arising in gas–solid two phase flow problems. The proposed scheme is then extended to the case of non-homogenous hyperbolic systems with a source term, in particular to the case of Euler equations with a gravitational source term. The obtained numerical results are in perfect agreement with corresponding ones appearing in the recent literature, thus confirming the efficiency and potential of the proposed method to handle both homogeneous and non-homogeneous hyperbolic systems.

1. Introduction

In this paper we develop a new unstaggered nonuniform central scheme (NUCS) for the numerical solution of general hyperbolic systems of conservation laws in one space dimension. Many problems arising in physics and engineering sciences can be formulated mathematically using hyperbolic systems of conservation laws [16,17,30] or, in the case of systems with a source term, hyperbolic systems of balance laws [29]. Such problems occur for example in aerodynamics, magnetohydrodynamics (MHD), hydrodynamics and many more. Central schemes are particularly attractive for solving hyperbolic systems as they avoid the resolution of the Riemann problems arising at the cell interfaces, thanks to a layer of staggered cells. Central schemes first appeared with the staggered version of Lax–Friedrichs's scheme, where a piecewise constant numerical solution was alternatingly evolved on two staggered grids. The resulting scheme is first-order accurate with a stability number of 0.5. In 1990 Nessyahu and Tadmor (NT) [19] presented a predictor-corrector type, second-order accurate scheme that is an extension of the Lax–Friedrichs scheme [14] which evolves a piecewise linear numerical solution on two staggered grids. The NT scheme uses a first-degree Taylor

* Corresponding author at: P.O. Box 13-5053 Chouran, Beirut: 1102 2801, Lebanon. +961 1 786456x1812. Tel.: +96 13834095.
E-mail address: rony.touma@lau.edu.lb (R. Touma).

http://dx.doi.org/10.1016/j.amc.2015.03.129
0096-3003/

expansion in time to determine the numerical solution at the intermediate time; furthermore slopes limiting reduces spurious oscillations in the vicinity of discontinuities. Multidimensional extension of the Nessyahu and Tadmor scheme for hyperbolic systems on staggered Cartesian grids and on unstructured grids were later developed and successfully used to solve problems primarily arising in aerodynamics [1,2,12,13,31,35]. Central schemes for ideal and shallow water magnetohydrodynamics were later developed in [32]. Recently, unstaggered central schemes (UCS) for hyperbolic systems on Cartesian grids were developed in [33] where the numerical solution is evolved on a single grid and the resolutions of the Riemann problems at the cell interfaces is by-passed thanks to a layer of ghost staggered cells. With the UCS scheme, additional treatment of the obtained numerical solution can be easily performed without any synchronization problem since the numerical solution is computed on a unique grid at any time (for example in the case of ideal/shallow water MHD/SMHD and shallow water equation problems SWE [32–34]).

In this paper, we extend the unstaggered central schemes [31,33] to the case of one-dimensional Cartesian and nonuniform grids. More specifically, we extend the unstaggered central scheme to solve a system of partial differential equations related to two-phase fluid flow problems. Within this context, it is widely accepted that two-phase flow equations are of highly nonlinear, non-hyperbolic and of non-conservative type as an initial-boundary-value problem leading to unstable solutions [20,26]. In general, there are two different theoretical formulations in two-phase flow: The mixture theory and the averaging based approaches [7,8,11]. Based on such approaches, there exist a large number of improved two-phase flow models available in the literature that have been used successfully leading to a well-posed initial-boundary-value problem; see for example [15,23,28,36] and reference therein. An issue of concern, however, related to such models is that they inherently have a non-conservative form due to the interaction between phases [25,27]. A recent approach is based on the formulation of thermodynamically compatible systems [9]. In such an approach the two-phase flow character is formulated in terms of parameters of the mixture (see for example [22]). The resulting system of PDEs is fully hyperbolic and fully conservative as an initial-boundary value problem and the current paper focuses on this type of systems. However, as known to all, analytical solutions to two-phase flow equations are limited to special cases of such flows [4]. This is due to the non-linearity and complicated nature of the governing equations of interest. Thus, numerical approaches have been widely applied to investigate two-phase flow equations. For such reasons, in the remainder of this paper, we focus on the numerical resolutions of a specific two-phase flow equations. Recently, thermodynamically compatible systems theory has been introduced for problems related to gas–solid tow-phase flows [21,38] together with Godunov finite volume methods for the Riemann problem associated with the model equations. Here we develop another resolution to the model equations proposed in [38] based on the current numerical scheme developed in this paper.

We then extend the proposed central scheme to the case of systems of gas dynamics with a gravitational term, more precisely to the case of Euler equations with a gravitational source term. This system is a nonhomogeneous hyperbolic system with a source term describing the effect of gravity on the fluid momentum and energy. The numerical base scheme will be generalized to the case of non-homogenous system in general, and specifically to the case of Euler equations with gravity in the case of non-steady flows. Several methods were recently developed for the numerical solution of systems of Euler equations with gravity including, among others, the essentially non-oscillatory (ENO) finite volume and finite difference schemes [10], the weighted ENO finite volume and finite difference schemes [18], and the discontinuous Galerkin methods [3].

The rest of the paper is organized as follows: In Section 2 we develop the unstaggered nonuniform extension of the original central schemes, and then, in Section 3, we extend the scheme to the case of non-homogenous systems. In Section 4 we briefly discuss the derivation of the two-phase flow equations and the Euler equations with a gravitational source term. The numerical validation of the developed scheme and some classical two-phase gas–solid flow problems and Euler systems with gravity are presented in Section 5. Concluding remarks are given in Section 6.

2. Unstaggered central schemes on nonuniform grids

We consider the initial value problem:

$$\begin{cases} u_t + f(u)_x = 0, \\ u(x, t=0) = u_0(x). \end{cases} \tag{1}$$

$u(x, t) = (u_1, u_2, \ldots, u_p)$ is the unknown p − components vector and $f(u)$ is the flux vector. System (1) is assumed to be hyperbolic, i.e., the Jacobian matrix $\partial f/\partial u$ has p real eigenvalues and p linearly independent eigenvectors [16,30]. We discretize the computational domain $[a, b]$ using n subintervals $C_i = [x_{i-1/2}, x_{i+1/2}]$ centered at the nodes x_i with different lengths Δx_i for $i = 1, \cdots, n$. The proposed numerical scheme evolves a piecewise linear numerical solution $L_i(x, t)$ defined at the centers x_i of the control cells C_i and we set $u_i^n = L_i(x_i, t^n)$ to be the cell centered value. The proposed scheme evolves the numerical solution on a unique grid with control cells C_i; however in order to avoid the resolution of the Riemann problems arising at the cell interfaces $x_{i\pm1/2}$, the numerical solution is first computed on the control dual cells $D_{ij} = [x_i, x_j]$ centered at x_{ij} with length Δx_{ij} and is then projected back onto the cells C_i. The geometry of the scheme is shown in Fig. 1. Without loss of generality we assume that the numerical solution u_i^n is known at time t^n at the center x_i of the cells C_i. The proposed scheme uses a piecewise linear reconstruction of the piecewise constant solution obtained at the previous time step:

$$u(x, t^n) \approx L_i(x, t^n) = u_i^n + (x - x_i)\left(u_i^n\right)', \ \forall x \in C_i, \tag{2}$$

where $(u_i^n)' \approx \frac{\partial}{\partial x} u(x, t^n)|_{x=x_i}$ approximates the slope to first-order accuracy. The solution of system (1) at time t^{n+1} is calculated as follows: We first integrate the conservation law in system (1) on the domain $R_{ij}^n = [x_i, x_j] \times [t^n, t^{n+1}]$ (shown in Fig. 2), and

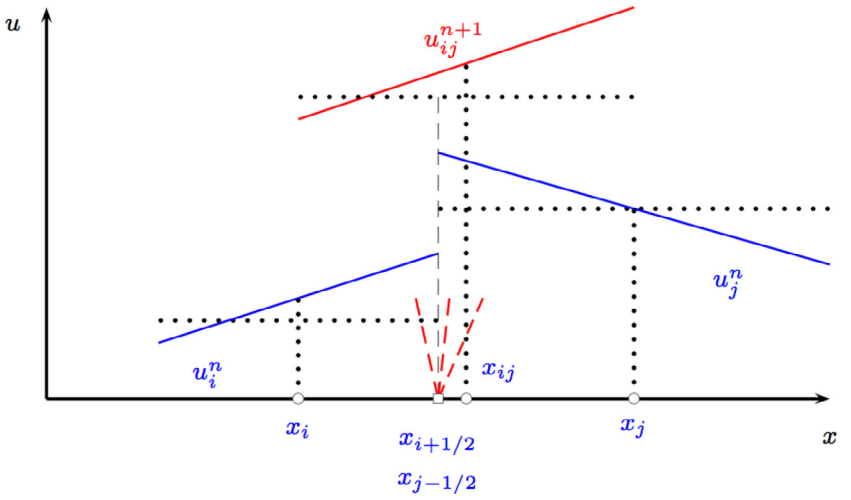

Fig. 1. Nonuniform domain decomposition of the proposed scheme: Two cells C_i and C_j and their corresponding dual cell D_{ij}.

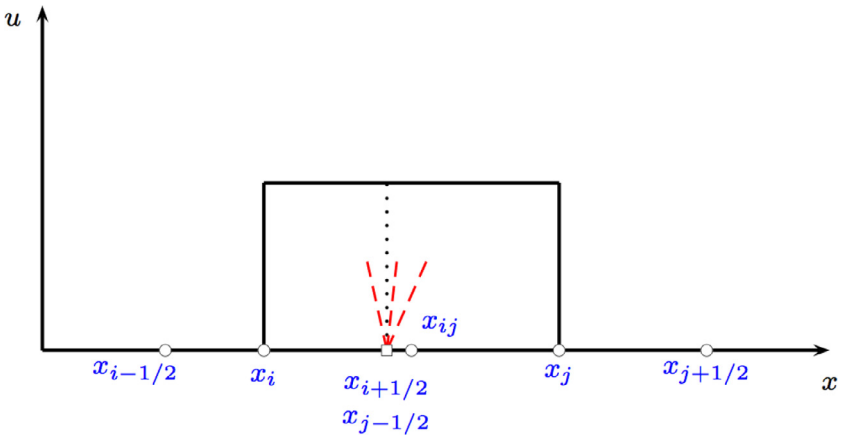

Fig. 2. Domain of integration R_{ij}^n.

then we apply Green's theorem

$$0 = \int_{R_{ij}^n} (u_t + f(u)_x)\, dA = \oint_{\partial R_{ij}^n} u\, dx - f(u)\, dt = \int_{x_i}^{x_j} u(x, t^n)\, dx + \int_{t^n}^{t^{n+1}} -f(u(x_j, t)\, dt + \int_{x_j}^{x_i} u(x, t^{n+1})\, dx + \int_{t^{n+1}}^{t^n} -f(u(x_i, t)\, dt. \tag{3}$$

Since, the numerical scheme evolves a piecewise linear numerical solution ($u(x, t) = L_i(x, t)\ \forall x \in C_i$), the integrals in (3) will be approximated with second-order of accuracy as follows:

$$\int_{x_i}^{x_j} u(x, t^{n+1})\, dx = \Delta x_{ij} u_{ij}^{n+1},$$

and

$$\int_{x_i}^{x_j} u(x, t^n)\, dx = \int_{x_i}^{x_{i+1/2}} u(x, t^n)\, dx + \int_{x_{j-1/2}}^{x_j} u(x, t^n)\, dx \approx \frac{\Delta x_i}{2} u_{i+1/4}^n + \frac{\Delta x_j}{2} u_{j-1/4}^n = \frac{\Delta x_i u_{i+1/4}^n + \Delta x_j u_{j-1/4}^n}{2}, \tag{4}$$

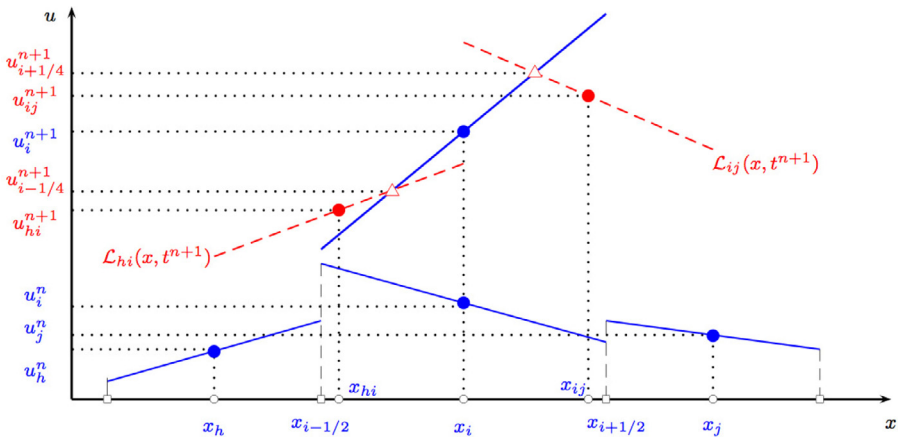

Fig. 3. Geometry of the projection step on the initial grid: linear interpolants through the points (x_{hi}, u_{hi}^{n+1}) and (x_{ij}, u_{ij}^{n+1}) are used to define the cell-centered solution u_i^{n+1}.

where the interpolated solution values at time t^n are obtained as follows

$$u_{i+1/4}^n = u_i^n + \frac{\Delta x_i}{4}\left(u_i^n\right)'.$$
$$u_{j-1/4}^n = u_j^n - \frac{\Delta x_j}{4}\left(u_j^n\right)'.$$

In this work we have mainly used a variant of van Leer's monotonized centered limiter (MC-θ) [37], where the numerical derivative $(u_i^n)'$ is calculated in terms of its neighboring values (shown in Fig. 3) as follows:

$$\left(u_i^n\right)' = \text{minmod}\left[\theta\frac{u_i^n - u_h^n}{\Delta x_{hi}}, D(u_h, u_i, u_j), \theta\frac{u_j^n - u_i^n}{\Delta x_{ij}}\right], \tag{5}$$

where θ is chosen such that $1 \le \theta \le 2$, and the minmod function is defined by

$$\text{minmod}\,(a, b, c) = \begin{cases} \text{sgn}(a)\cdot\min\{|a|, |b|, |c|\}, & \text{if } a,\ b,\ c \text{ have the same sign} \\ 0 & \text{otherwise.} \end{cases} \tag{6}$$

Other limiters may also be used to estimate the numerical derivative.

The term $D(u_h, u_i, u_j)$ in Eq. (5) denotes a three point derivative approximation obtained using the method of variable coefficients and is defined as follows:

$$D(u_h, u_i, u_j) = -\frac{h_2}{h_1(h_1+h_2)}u_h^n + \left(\frac{h_2}{h_1(h_1+h_2)} - \frac{h_1}{h_2(h_1+h_2)}\right)u_i^n + \frac{h_1}{h_2(h_1+h_2)}u_j^n \tag{7}$$

with $h_1 = x_i - x_h$ and $h_2 = x_j - x_i$. To approximate the time integrals in Eq (3) with a second-order of accuracy we follow a predictor-corrector integration technique as follows:

$$\int_{t^n}^{t^{n+1}} f(u(x_i, t))\,dt \approx \Delta t f\left(u_i^{n+1/2}\right). \tag{8}$$

$$\int_{t^n}^{t^{n+1}} f(u(x_j, t))\,dt \approx \Delta t f\left(u_j^{n+1/2}\right). \tag{9}$$

where the solution value at the intermediate time is obtained using a first-order Taylor expansion in time as well as the hyperbolic conservation law as follows:

$$\begin{aligned} u(x_i, t^{n+1/2}) &\cong u(x_i, t^n) + \frac{\Delta t}{2}u_t(x_i, t^n) \\ &\cong u_i^n - \frac{\Delta t}{2}f(u)_x|_{(x_i, t^n)} \\ &\cong u_i^n - \frac{\Delta t}{2}f'\left(u_i^n\right)\left(u_i^n\right)' \equiv u_i^{n+1/2}. \end{aligned} \tag{10}$$

Here $f'(u)$ is the derivative of the flux function with respect to u, and $(u_i^n)'$ is the limited spatial numerical derivative of the solution previously obtained using Eq. (5).

The solution u_{ij}^{n+1} at time t^{n+1} can now be defined on the staggered dual cell D_{ij} as follows:

$$u_{ij}^{n+1} = \frac{\Delta x_i u_i^n + \Delta x_j u_j^n}{2\Delta x_{ij}} + \frac{(\Delta x_i)^2 (u_i^n)' - (\Delta x_j)^2 (u_j^n)'}{8\Delta x_{ij}} - \frac{\Delta t}{\Delta x_{ij}} \left(f\left(u_j^{n+1/2}\right) - f\left(u_i^{n+1/2}\right)\right). \tag{11}$$

A projection step of u_{ij}^{n+1} back onto the cells C_i is required to define the solution u_i^{n+1}. Since, the numerical solution is defined using piecewise linear reconstructions of the piecewise constant solution defined at the center of the cells C_i and D_{ij}, we first define the piecewise linear reconstructions on the dual cells D_{hi} and D_{ij} as follows:

$$\mathcal{L}_{hi}(x, t^{n+1}) = u_{hi}^{n+1} + (x - x_{hi}) \left(u_{hi}^{n+1}\right)', \tag{12}$$

$$\mathcal{L}_{ij}(x, t^{n+1}) = u_{ij}^{n+1} + (x - x_{ij}) \left(u_{ij}^{n+1}\right)', \tag{13}$$

with $0 < |x - x_{hi}| < \Delta x_{hi}/2, 0 < |x - x_{ij}| < \Delta x_{ij}/2$, and where $(u_{hi}^{n+1})'$ and $(u_{ij}^{n+1})'$ denote the limited numerical derivatives associated with the piecewise linear interpolants on the dual cells D_{hi} and D_{ij}, respectively. We then define the solution values u_i^{n+1} (figure 3) at the center of the cell $C_i = [x_{i-1/2}, x_{i+1/2}]$ using the formula:

$$u_i^{n+1} = L_i(x_i, t^{n+1}),$$

where $L_i(x, t^{n+1})$ is the piecewise linear numerical solution defined on control C_i and going through the points $(x_{i-1/4}, \mathcal{L}_{hi}(x_{i-1/4}, t^{n+1}))$, (x_i, u_i^{n+1}), and $(x_{i+1/4}, \mathcal{L}_{ij}(x_{i+1/4}, t^{n+1}))$ and is given by:

$$L_i(x, t^{n+1}) = \mathcal{L}_{hi}(x_{i-1/4}, t^{n+1}) + \frac{\mathcal{L}_{ij}(x_{i+1/4}, t^{n+1}) - \mathcal{L}_{hi}(x_{i-1/4}, t^{n+1})}{(\Delta x_i)/2}(x - x_{i-1/4}), \tag{14}$$

$$L_i(x, t^{n+1}) = \mathcal{L}_{ij}(x_{i+1/4}, t^{n+1}) + \frac{\mathcal{L}_{ij}(x_{i+1/4}, t^{n+1}) - \mathcal{L}_{hi}(x_{i-1/4}, t^{n+1})}{(\Delta x_i)/2}(x - x_{i+1/4}), \tag{15}$$

where $\mathcal{L}_{hi}(x, t^{n+1})$ and $\mathcal{L}_{ij}(x, t^{n+1})$ are the piecewise linear reconstructions of u_{hi}^{n+1} and u_{ij}^{n+1} on the dual cell D_{hi} and D_{ij} obtained using Eqs. (12)–(13).

Using Eq. (14) (or Eq. (15)), we can now define the solution u_i^{n+1} at the center of the control cell C_i as follows:

$$u_i^{n+1} = L_i(x_i, t^{n+1}) = \frac{1}{2}(u_{hi}^{n+1} + u_{ij}^{n+1}) + \frac{\Delta x_h}{8}(u_{hi}^{n+1})' - \frac{\Delta x_j}{8}(u_{ij}^{n+1})'. \tag{16}$$

Finally, we note that the stability condition of the proposed method follows the one presented in [19] and the time step Δt is dynamically calculated using the wave speed and the minimum cell length value $\Delta x = \min_k(\Delta x_k)$.

3. Central schemes for non-homogenous hyperbolic systems

The finite volume scheme presented is Section 2 can be extended to the case of non-homogeneous hyperbolic systems with a source term of the form:

$$\begin{cases} \mathbf{u}_t + f(\mathbf{u})_x = S, \\ \mathbf{u}(x, t = 0) = \mathbf{u}_0(x). \end{cases} \tag{17}$$

where $\mathbf{u}(x, t)$, is the unknown vector, $f(\mathbf{u})$ is the flux function, and S is the source term that depends on $\mathbf{u}$ and possibly on the spacial variable x (geometrical source term). Assuming an approximation $(\mathbf{u}_i^n)$ to the solution of 17 is known at time t^n on the cells C_i, the solution at the next time step $t^{n+1} = t^n + \Delta t$ is calculated by following the same strategy presented in Section 2: We start by integrating the PDE in Eq. (17) on R_{ij}^n, we apply Green's theorem to the integral to the left and we solve for $\mathbf{u}_{ij}^{n+1}$; we obtain:

$$\mathbf{u}_{ij}^{n+1} = \frac{\Delta x_i \mathbf{u}_i^n + \Delta x_j \mathbf{u}_j^n}{2\Delta x_{ij}} + \frac{(\Delta x_i)^2 (\mathbf{u}_i^n)' - (\Delta x_j)^2 (\mathbf{u}_j^n)'}{8\Delta x_{ij}} - \frac{\Delta t}{\Delta x_{ij}} \left(f\left(\mathbf{u}_j^{n+1/2}\right) - f\left(\mathbf{u}_i^{n+1/2}\right)\right) + \frac{1}{\Delta x_{ij}} \int_{R_{ij}^n} S \, dA \tag{18}$$

The integral of the source term is approximated with second-order of accuracy using the midpoint quadrature rule using predicted solution values obtained at time $t^{n+1/2}$ using Taylor series expansions as follows:

$$\int_{R_{ij}^n} S \, dA \approx S\left(\mathbf{u}_i^{\mathbf{u}+1/2}, \mathbf{u}_j^{n+1/2}, x_i, x_j\right) \tag{19}$$

As in Eq. (10), the solution's predicted values $u_i^{n+1/2}$ are obtained as follows:

$$\mathbf{u}_i^{n+1/2} = \mathbf{u}_i^n + \frac{\Delta t}{2}\left[-f'\left(\mathbf{u}_i^n\right)\left(\mathbf{u}_i^n\right)' + S\left(\mathbf{u}_i^n, x_i\right)\right] \tag{20}$$

where $S(u_i^n, x_i)$ discretizes the source term at time t^n on the cells C_i. In Section 6 we shall adapt the proposed central scheme to the case of Euler equations with a gravity source term and solve some classical problems.

4. Applications

To validate our developed scheme we shall consider classical problems arising in gas–solid two phase flow problems and gas dynamics with and without gravity/friction source terms as we shall see in the following subsections.

4.1. Two-phase gas–solid flows

Two phase gas–solid flows are widely applied in industry, including petroleum, chemical, metallurgical and energy industries. The governing flow field equations in terms of parameters of state for the mixture consists of balance laws for mass, momentum and energy along with additional closure governing equations. In one-dimensional space, these are given as follows [38,39]:

- mixture mass

$$\frac{\partial(\rho)}{\partial t}+\frac{\partial(\rho u)}{\partial x}=0, \tag{21}$$

- mixture momentum

$$\frac{\partial(\rho u)}{\partial t}+\frac{\partial(\rho u^2+P)}{\partial x}=0, \tag{22}$$

- mixture energy

$$\frac{\partial(\rho E)}{\partial t}+\frac{\partial(\rho uE+Pu)}{\partial x}=0, \tag{23}$$

where t is the time and x is the spatial coordinate that describes the flow direction. ρ, u, P and E are the density, velocity, pressure and the energy for the gas–solid mixture, respectively. Furthermore, the above system is completed by three equations that allow phase interaction between the gas and the solid phases. Thus, the following system accounts for the gas volume concentration, α, mass gas concentration, c, and gas entropy concentration χ:

- gas volume concentration

$$\frac{\partial(\rho\alpha)}{\partial t}+\frac{\partial(\rho u\alpha)}{\partial x}=\phi, \tag{24}$$

- mass gas concentration

$$\frac{\partial(\rho c)}{\partial t}+\frac{\partial(\rho uc)}{\partial x}=\psi, \tag{25}$$

- gas entropy concentration

$$\frac{\partial(\rho\chi)}{\partial t}+\frac{\partial(\rho u\chi)}{\partial x}=\omega. \tag{26}$$

The source terms appearing in Eqs. (24)–(26) describe the interphase exchange processes that accounts for the pressure relaxation, mass exchange and energy exchange [6].

For a complete description of the forgoing equations (i.e. Eqs. (21)–(26)) and for our particular situation of gas–solid mixture, the equations of state for both phases and the mixture are needed. To start with equation of state for the gas, we employ the equation of perfect gas of [21,38]:

$$e_1=\frac{A_0}{\rho_1^0(\gamma-1)}\left(\frac{\rho}{\rho_1^0}\right)^{\gamma-1}exp\left(\frac{s}{c_{v1}}\right), \tag{27}$$

where the subscript 1 denotes the gas phase and $\gamma=1.4$, $\rho_1^0=1$, $c_v^1=720$ and $A_0=1\times10^5$. Further, the Mie–Gruneisen equation of state [21] is considered for the solid phase:

$$e_2=\frac{A_1^2}{2A_2^2}\left[\left(\frac{\rho}{\rho_2^0}\right)^{A_2}-1\right]^2+c_{v2}A_3\left(\frac{\rho}{\rho_2^0}\right)^{A_4}\left[exp\left(\frac{s}{c_v^2}\right)-1\right]-\frac{A_5}{\rho}, \tag{28}$$

where 2 stands for the solid phase and the constants are taken as: $\rho_2^0=2.77$, $c_v^2=0.00045$, $A_1=6$, $A_2=1.08$, $A_3=293$, $A_4=2.11$ and $A_5=0.1$. In the context of two-phase mixtures, an equation of state for gas–solid mixture is obtained using the above equations of state by the following formula [38]:

$$e=ce_1+(1-c)e_2 \quad \text{with} \quad c=\frac{\alpha\rho_1}{\rho}, \tag{29}$$

where ρ_1 is the gas phase density and the volume concentrations satisfy the relation: $\alpha+(1-\alpha)=1$. Further, formula (29) leads to the following relation for mixture pressure computation [22,38]

$$P=\rho^2\frac{\partial e}{\partial\rho}. \tag{30}$$

The time-dependent model equations in (21)–(26) can be written in the form

$$\frac{\partial \mathbf{u}}{\partial t} + \frac{\partial f(\mathbf{u})}{\partial x} = S(\mathbf{u}), \quad t \in \mathbb{R}^+, -\infty < x < \infty, \tag{31}$$

where

$$\mathbf{u} = \begin{pmatrix} \rho \\ \rho u \\ \rho E \\ \rho \alpha \\ \rho c \\ \rho \chi \end{pmatrix}, \quad f(\mathbf{u}) = \begin{pmatrix} \rho u \\ \rho u^2 + P \\ \rho u E + P u \\ \rho u \alpha \\ \rho u c \\ \rho u \chi \end{pmatrix}, \quad S(f) = \begin{pmatrix} 0 \\ 0 \\ 0 \\ \phi \\ \psi \\ \omega \end{pmatrix}. \tag{32}$$

Together with (27), (28) and (29), system (31) constitute six equations in six unknowns for the mixture and phases. Further, system (31) can be solved provided that appropriate initial and boundary conditions are supplied. Finally, theoretical analyses have shown the eigenvalues of the Jacobian of the flux vector of system (21)–(26) are given unconditionally by:

$$\lambda_1 = u - a_m, \quad \lambda_{2,3,4,5} = u, \quad \lambda_6 = u + a_m, \tag{33}$$

where a_m stands for the speed of sound of the system. The eigenvalues λ_1 and λ_6 are associated with the acoustic waves speed propagation, while the eigenvalues $\lambda_{2,3,4,5}$ represent the velocity of the particle. We refer the reader to [38] for further details to the mathematical structure and physical properties of the current model equations and to [22] for comparisons with other two-phase flow models.

4.2. Euler equations with gravity

Many physical phenomena are modeled using the Euler equations with a gravitational source term, such as the study of atmospheric problems, weather predictions, climate modeling in addition to problems in astrophysics such as solar climate and simulations of supernova blasts. The Euler equations with gravitational source terms describe the conservation of mass, momentum and energy. Written in their conservative form the Euler equations with gravity are

$$\mathbf{u}_t + f(\mathbf{u})_x = S, \tag{34}$$

where $\mathbf{u} = (\rho, \rho v, \rho E)$, $f(\mathbf{u}) = (\rho v, \rho v^2 + P, \rho v E + P v)$, and $S = (0, \rho g - \alpha \rho v, \rho v g - \alpha \rho v^2)$.

Here t is the time and x is the spatial coordinate. ρ denotes the fluid density, v is its velocity and ρE is the total energy. P denotes the pressure and is given by the equation of state $P = (\gamma - 1)\rho\varepsilon$ with $E = \varepsilon + v^2$ The constants α and g denote the friction coefficient and the gravitational constant, respectively. When applying the applying the proposed scheme to system (34) and in the absence of friction, we discretize the integral of the source term in Eq. (19) with second-order of accuracy as follows:

$$\int_{R_{ij}^n} S \, dA \approx \Delta t \Delta x_{ij} \begin{pmatrix} 0 \\ \dfrac{\rho_i^{n+1/2}\Delta x_i + \rho_j^{n+1/2}\Delta x_j}{\Delta x_{ij}} g \\ \dfrac{\rho_i^{n+1/2}\Delta x_i + \rho_j^{n+1/2}\Delta x_j}{\Delta x_{ij}} \dfrac{v_i^{n+1/2}\Delta x_i + v_j^{n+1/2}\Delta x_j}{\Delta x_{ij}} g \end{pmatrix} \tag{35}$$

We note here that the discretization in equation can be used in the case of non-steady two-phase flows.

The predicted solution values at time $t^{n+1/2}$ obtained using Eq. (20) involve the discretization of the source term at time t^n on the control cells C_i. We propose the following discretization:

$$S(\mathbf{u}_i^n) \approx \begin{pmatrix} 0 \\ \rho_i^n g \\ \rho_i^n v_i^n g \end{pmatrix} \tag{36}$$

Eqs. (35) and (36) can now be used to update the solution at time t^{n+1} in Eq. (18) in order to define the staggered solution values u_{ij}^{n+1}. The numerical solution at time t^{n+1} on the control cells C_i will be obtained using the back projection step defined in Eq. (16).

5. Numerical experiments

In this section we assess the performance of the proposed scheme for the system of fully hyperbolic conservative two-phase flow equations introduced in [6] for compressible gas–solid mixtures.

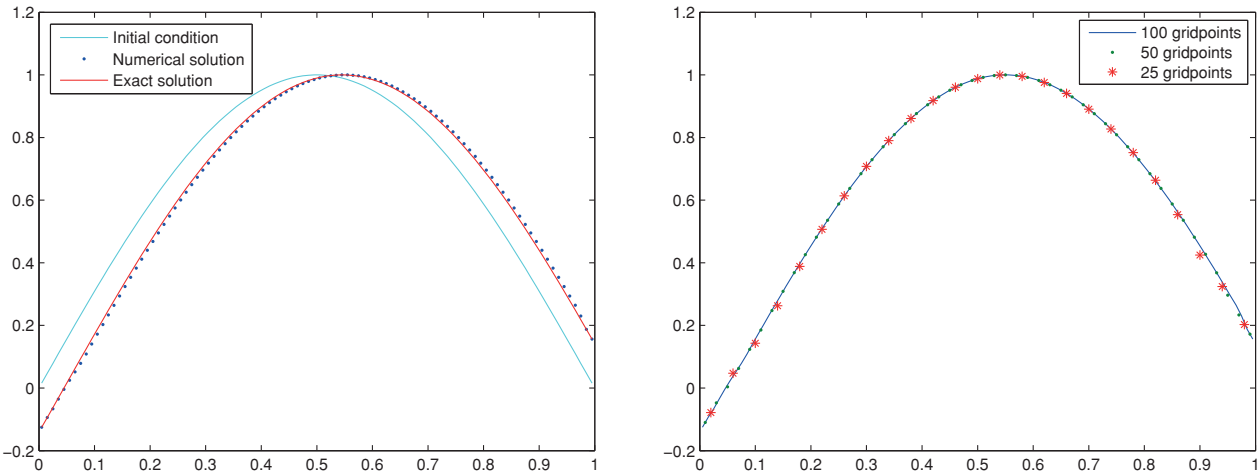

Fig. 4. Linear advection problem: (Left) Numerical solution obtained using the proposed unstaggered nonuniform scheme (dotted curve) and is compared to the exact solution (solid curve); (right) numerical solution obtained on 25, 50, and 100 gridpoints.

Table 1
Errors and orders of convergence on the linear advection problem with $u_0(x) = \sin(\pi x)$.

Grid size	L_2 error	L_2 order
20	0.1233	-
40	0.0338	1.8670
80	0.0090	1.9074

5.1. Testcase 1: linear advection and numerical convergence

Before considering gas–solid two-phase flow problems, we first validate our developed numerical scheme by considering a simple scalar advection problem given by:

$$\begin{cases} u_t + u_x = 0, \\ u(x,t)|_{t=0} = u_0(x). \end{cases} \tag{37}$$

The analytic exact solution of system (37) at the space-time point (x, t) is obtained from the initial data as $u(x, t) = u_0(x - t)$. We consider for our computational domain the interval $[0, 1]$ discretized with 100 gridpoints. The length Δx_i of each control cell C_i lies in the interval $[0.005, 0.02]$. The initial data function is given by $u_0(x) = \sin(\pi x)$.

Fig. 4 shows the curves of the initial data, the numerical solution (dotted curve) and the exact solution (solid curve) obtained at the final time $t_f = 0.5$.

Next, we validate the order of convergence of the proposed scheme and calculate the L_2-errors and the order of convergence. The obtained results reported in Table 1 confirm the order of the proposed scheme.

5.2. Testcase 2: sod shock tube problem

Now we apply the proposed scheme and solve the classical gas dynamics Sod shock-tube problem [24]. The initial data for this test features a shock across the point $x = 0.5$; the two constant states are $U_l = [1, 0, 1]$ (if $0 < x < 0.5$) and $U_r = [0.125, 0, 0.1]$ (if $0.5 < x < 1$) for $U = [\rho, \rho u, \rho e]$. The adiabatic constant is $\gamma = 1.4$. The computational domain $0 \le x \le 1$ is discretized using 200 gridpoints and the numerical solution is computed at time $t = 0.164$ using the proposed scheme. A comparison between the obtained results and the exact solution is shown in Fig. 5. The results shown in Fig. 5 show an excellent agreement between the computed numerical results and the exact solution. Fig. 6 shows the profile of the mass density obtained using the unstaggered central scheme on structured cells, the unstaggered central scheme on nonuniform cells with the Venkatakrishnan limiter and the Minmod limiter. As is shown in Fig. 6 these curves are in good agreement with the reference/exact solution obtained on 3000 cells.

5.3. Testcase 3: multiphase gas–solid problems

In this section, we apply the proposed numerical scheme and simulate four gas–solid two-phase mixtures test cases.

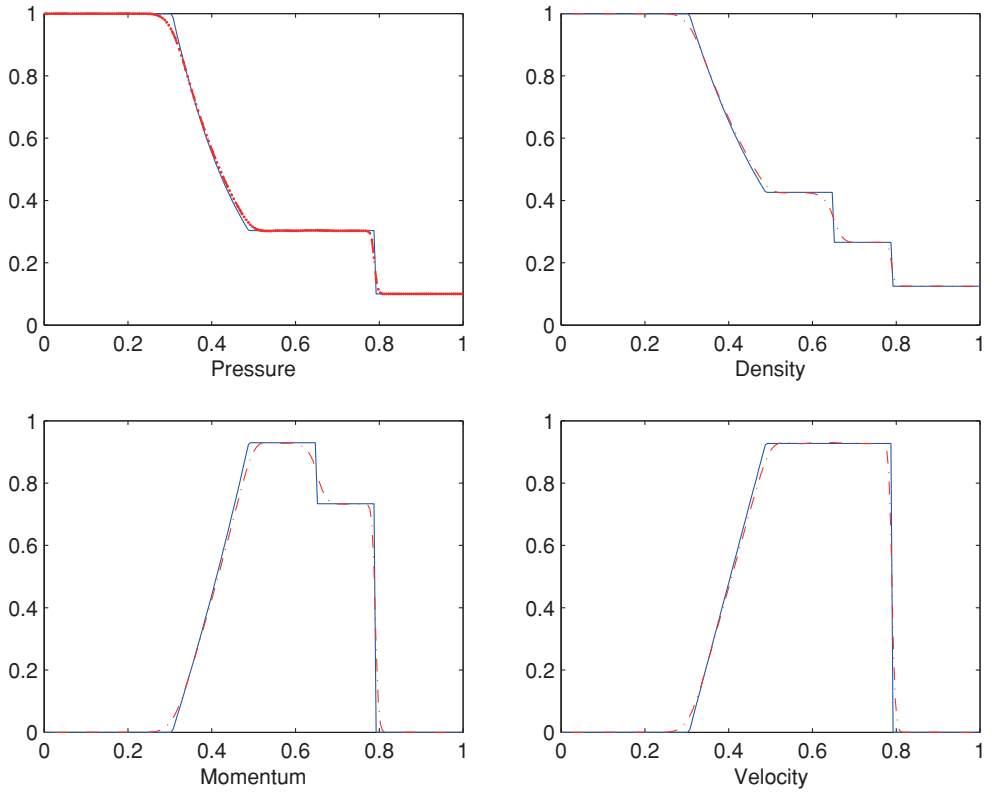

Fig. 5. Sod shock-tube problem: numerical solution (dotted curves) and reference solution (solid curves) of the gas dynamics shock-tube problem.

The four configurations are solved using system (21)–(26) of Section 4. Furthermore, all the provided numerical results are thoroughly compared with the reference solutions produced using the total variation diminishing (TVD) slope limiter center (SLIC) scheme [38] which belongs to Godunov methods of centered type.

5.3.1. Configuation 1

This test case is dedicated to volume wave propagation within a gas–solid mixture of [38]. The initial data is made of two states defined by $U_l = [100, 0, 0, 0, 0,]$ if $x < 0$, and $U_r = [50, 1, 0, 0, 0,]$ if $x > 0$, where $U = [\rho, \alpha, u, \chi, s]$. The computational domain $[-10, 10]$ is discretized using 200 gridpoints. The exact solution to this problem consists of a left rarefaction wave and a right shock wave separated by a multiple contact discontinuity located at $x = 0$. The solution is computed at the time $t = 0.01$. The results are displayed in Fig. 8 using the proposed nonuniform central scheme with the minmod limiter. Fig. 7 shows results for the mixture density, mixture velocity, mixture pressure and volume concentration. The results are compared with the reference solution obtained using the SLIC scheme of [38]. An excellent agreement between the results obtained using the proposed scheme and those of the SLIC methods is observed in Fig. 8. It suggests that the present numerical procedure is very robust, even at severe conditions for the volume concentration, $(\alpha_L, \alpha_R) = (0.0, 1.0)$ with no spurious overshoots or oscillations. As observed in Fig. 8, the complete wave structure is completely reproduced as the reference solution using a coarse grid of cells. All waves are well resolved and generally accepted in the present literature [38] as correct.

5.3.2. Configuration 2: gas–solid mixture collision

This test features a collision of a gas–solid mixture: the initial data is given by $U_l = [0.1, 0.1, 800, 0, 0]$ and $U_r = [0.1, 0.1, -800, 0, 0]$ where $U = [\rho, \alpha, u, \chi, s]$ and c calculated using (29) with the gas phase density $\rho_{1L} = 1 = \rho_{1R}$. The computational domain is the interval $[0, 1]$ and the Riemann problem is set at the point $x_0 = 0.5$ with $u = U_l$ if $x \le x_0$ and $u = U_r$ otherwise. The exact solution to this problem features two strong fast shock waves propagating symmetrically in opposite directions separated by a multiple contact discontinuity about the point x_0. Fig. 9 shows the solution curves obtained using the proposed nonuniform central scheme (dotted curve); the reference solution (solid line) is obtained using the scheme presented in [38] on 5000 gridpoints. The obtained numerical results for the mixture density ρ, velocity u, mass gas concentration c, and the mixture temperature T_m are shown in Fig. 9 along with the corresponding reference solutions; the obtained results show a perfect agreement, thus confirming the efficiency and potential of the proposed scheme.

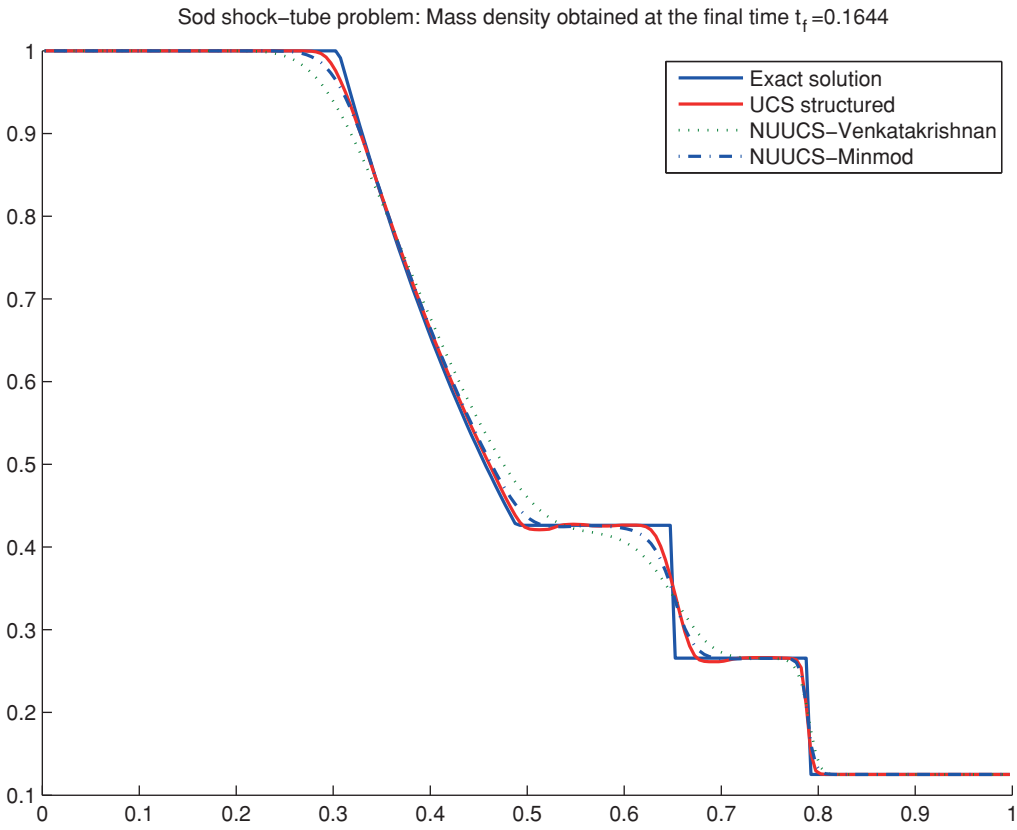

Fig. 6. Sod shock-tube problem: numerical solution (dotted curves) and reference solution (solid curves) of the gas dynamics Sod shock-tube problem.

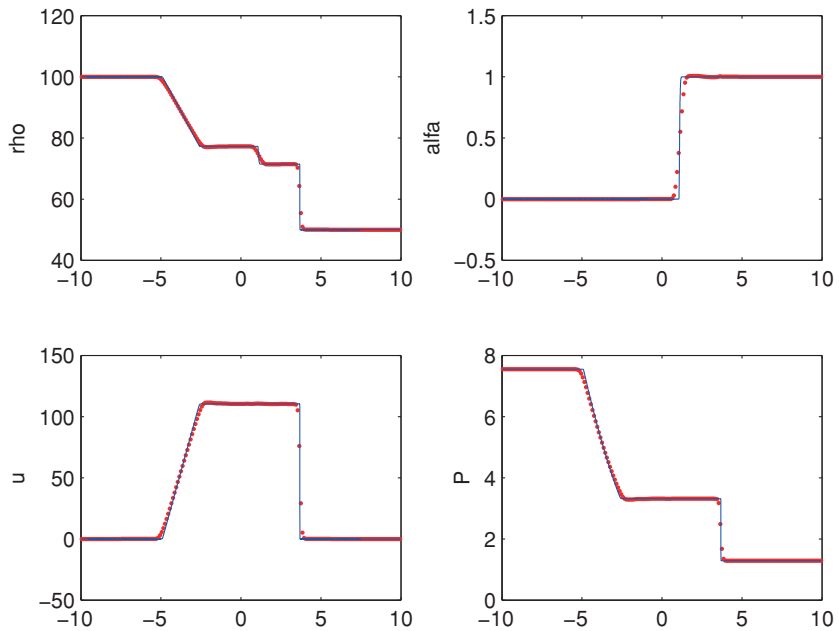

Fig. 7. Configuration 1: numerical solution (dotted curves) and reference solution (solid curves) of the first gas–solid two phase flow problem.

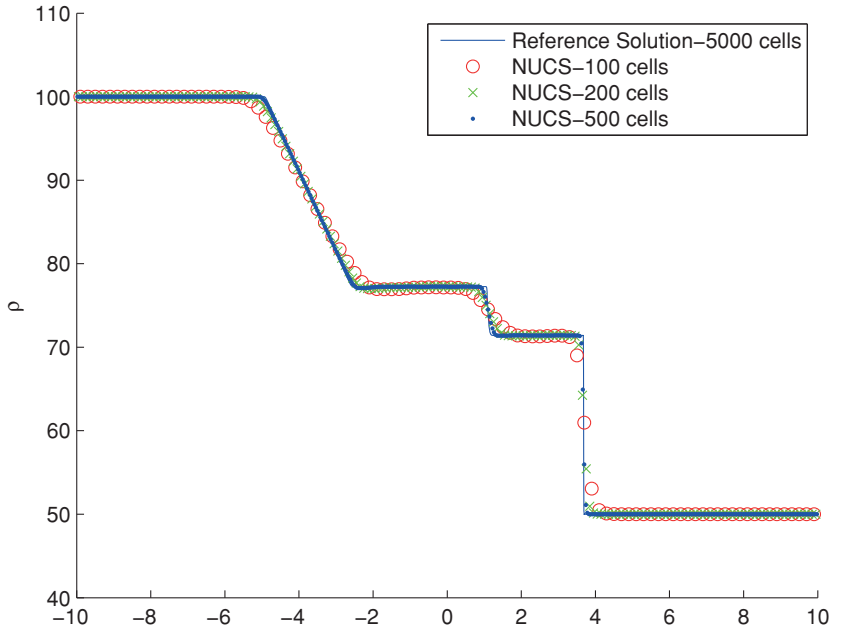

Fig. 8. Configuration 1: profile of the mass density obtained using the NUCS scheme on 100, 200 and 500 cells; the reference solution (solid line) is obtained using the SLIC scheme on 5000 cells.

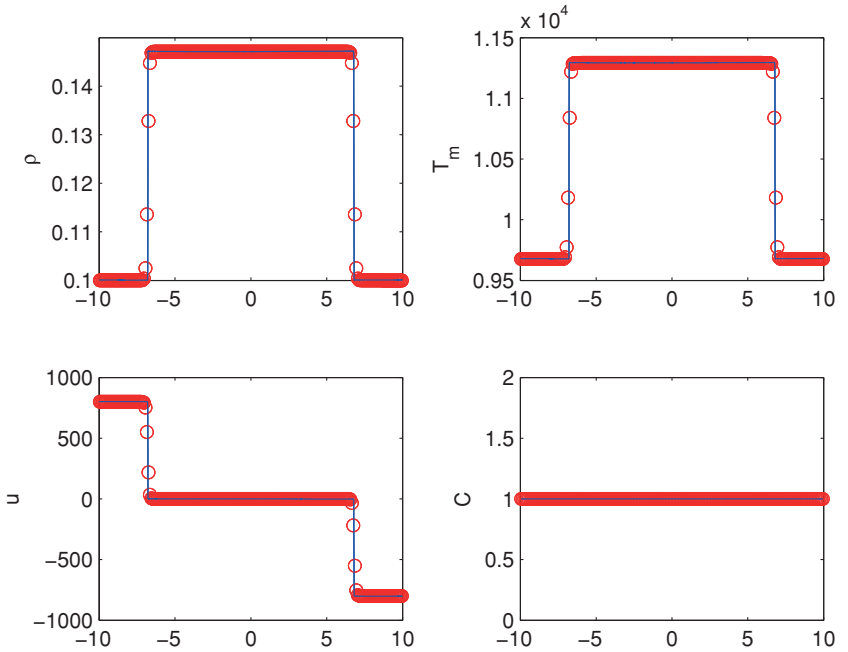

Fig. 9. Configuration 2: numerical solution (dotted curves) and reference solution (solid curves) of the gas–solid mixture collision two-phase flow problem.

5.3.3. Configuration 3: rarefaction waves within gas–solid mixture

This test case is an idealization of the rarefaction waves propagation within gas–solid mixtures described in [38]. The overall feature of this test case is similar to the cavitation tube with a non-trivial multiple contact discontinuity. The initial data for this particular test case are: $U = U_l = [70, 0.95, -100, 0, 0]$ for $x < 0$ and $U = U_r = [70, 0.05, 100, 0, 0]$ for x>0, where $u = [\rho, \alpha, u, \chi, s,]$ and c calculated using (29) as indicated in the previous test case. The computational domain $-10 \le x \le 10$ is discretized using 200 gridpoints and the numerical solution is calculated at the final time $t = 1.5$. Fig. 10 shows the reference solution (solid curves) of [38] and the numerical solution (dotted curves) obtained at time $t = 1.5$ using the proposed NUCS scheme. The results of the mass density ρ, the velocity u and the gas phase temperature T_2 show two critical left and right propagating rarefaction waves separated by a strong non-trivial multiple contact discontinuity which is due to the different values of the gas volume

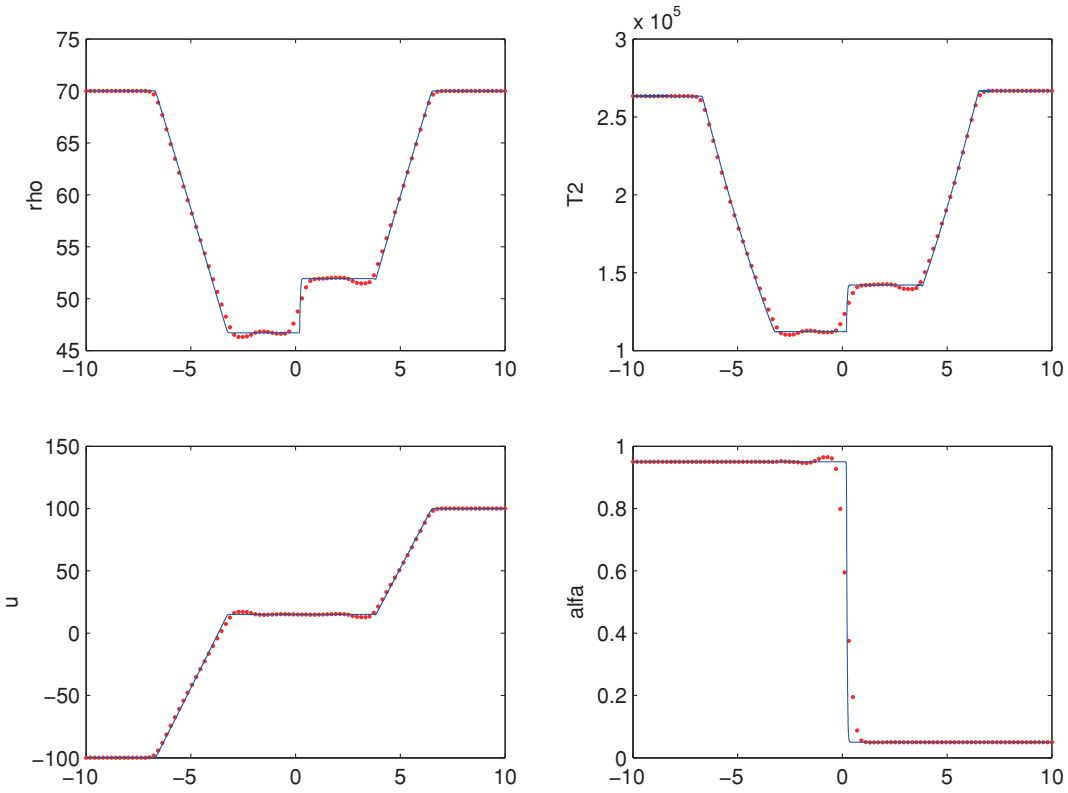

Fig. 10. Configuration 3: numerical solution (dotted curves) and reference solution (solid curves) of the rarefaction waves propagation in gas–solid mixture problem.

concentration on the left and right given data. Fig. 10 clearly shows that there exists a long expansion within the left rarefaction wave of the velocity profile. This velocity profile, however, indicates that there is a strong effect of the gas volume concentration on the complete wave structure. It is clear that the proposed NUCS method properly captures the whole wave structure and reproduces the left and right tails of both rarefactions. The obtained numerical results show a very good agreement with the reference solution (calculated on 5000 gridpoints) provided in [38] which is based on Godunov type methods and free of spurious oscillations associated with the non-trivial multiple contact discontinuity. However, the over and under shoots appearing near the jumps and shock waves will always appear when central schemes are involved. They are mainly due to the gradient limiting process. Finally, these results illustrate the efficiency and potential of the proposed NUCS method for implementation in finite volume techniques on nonuniform grids.

5.3.4. Configuration 4: two-phase flow dam break problem

For our last experiment we consider an adaptation of the classical hydrodynamics dam break problem [5,33] to the case of gas–solid two-phase flows. The initial data features an inner state $U_{in} = [100, 0, 0, 0, 0]$ defined over the interval $-1 \le x \le 1$ and an outer space $U_{out} = [50, 0, 0, 0, 0]$ elsewhere in the computational domain $-10 \le x \le 10$, where $U = [\rho, \alpha, u, \chi, s]$. The numerical solution is calculated at the final time $t = 0.2538$ on 200 gridpoints using the nonuniform unstaggered central scheme. Fig. 11 shows the profiles of ρ, α, u, and c at time $t = 0.05$ obtained on 100 gridpoints (dotted curve), 200 gridpoints (dashed curve), and 400 gridpoints (solid curve). Fig. 12 shows several plots of the mass density at different times and shows the symmetric propagation of the shock waves and rarefaction waves outwards.

5.4. Euler equations with a gravitational source term

The developed scheme is now extended to the case of Euler equations with a gravitational source term of Section 4. Two problems are considered the SOD shock-tube problem and Toro's dam break problem. The obtained results show the effects of the gravitational field on the structure of the solution of each problem.

5.4.1. Sod shock-tube problem with gravity

We consider here the Sod shock-tube problem solved under a gravitational field using the same initial data as in Section 5.2; however here we include the source term $S = (0, \rho g - \alpha\rho v, \rho v g - \alpha\rho v^2)$ with $g = 9.81$ is the gravitational constant and α denotes the friction coefficient. The computational domain $0 \le x \le 1$ is discretized using 200 gridpoints and the initial two constant states are $U_l = [1, 0, 2.5]$ for $0 \le x \le 0.5$ and $U_r = [0.125, 0, 0.025]$ for $0.5 \le x \le 1$ where $U = [\rho, v, p]$.

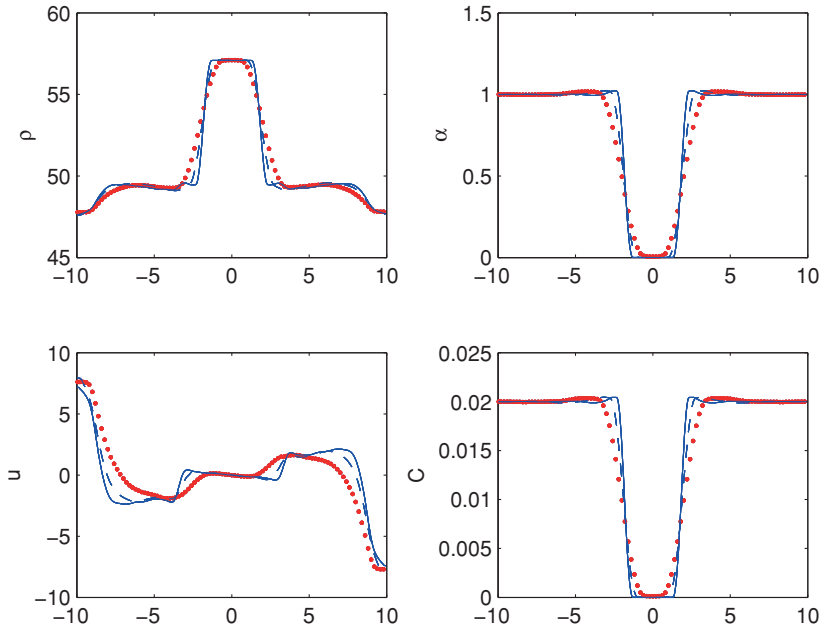

Fig. 11. Configuration 4: numerical solution of the dam-break gas–solid two-phase flow problem obtained using the NUCS method at time $t = 0.05$ obtained on 100 gridpoints (dotted curve), 200 gridpoints (dashed curve), and 400 gridpoints (solid curve).

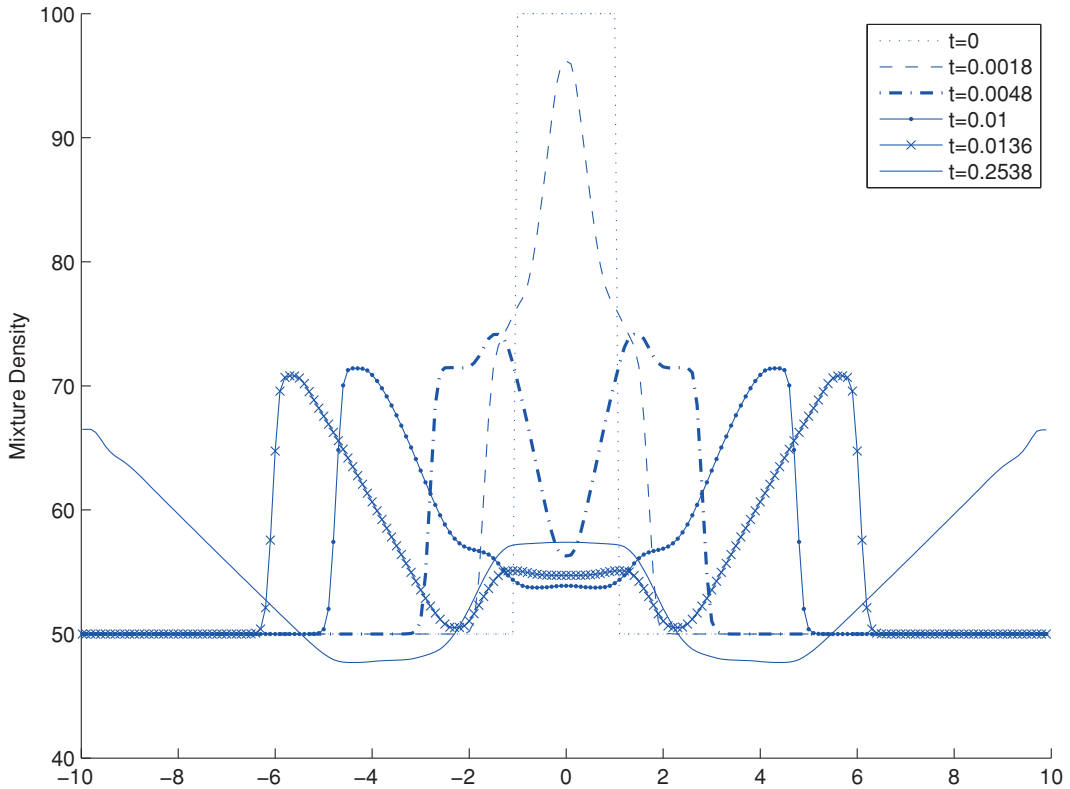

Fig. 12. Configuration 4: profile of the mass density of the dam-break gas–solid two-phase flow problem at different times.

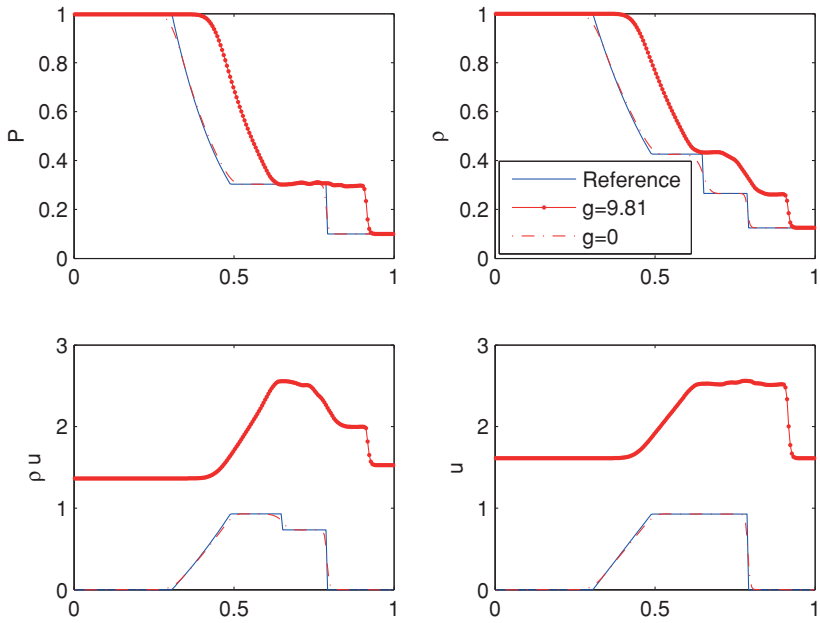

Fig. 13. Sod shock tube problem with and without gravity: profile of the pressure p, mass density ρ, momentum ρv, and velocity v obtained at the final time $t_f = 0.1644$.

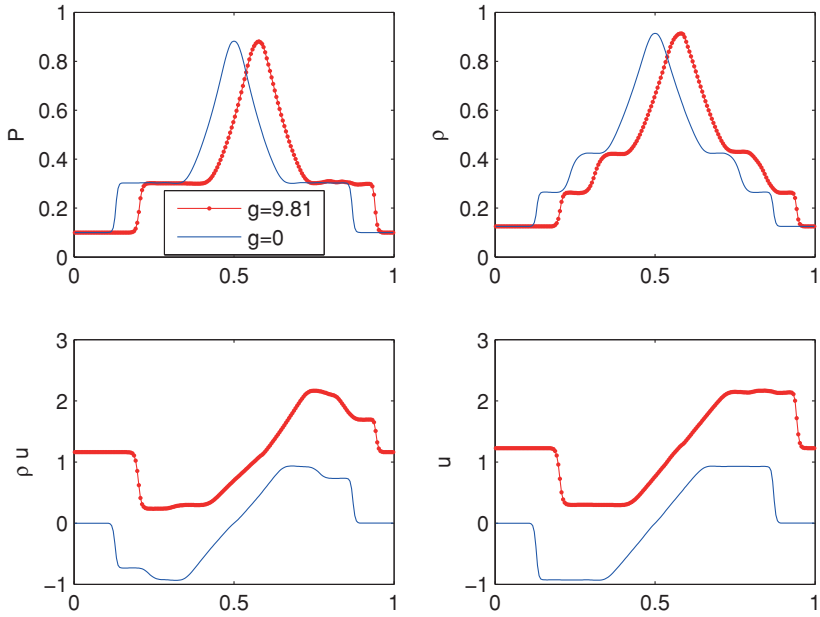

Fig. 14. Toro's dam break problem with and without gravity: profile of the pressure p, mass density ρ, momentum ρv, and velocity v obtained at the time $t = 0.125$.

The solution is computed at the final time time $t = 0.1644$ using the numerical scheme presented in Section 3. The numerical solution computed on a 200 grid and is shown in Fig. 13 (dotted curve). The reference solution (solid curve) shown in Fig. 13 is "exact" solution of the shock tube problem (with zero gravity) obtained on 200 gridpoints, and the dashed curve is the solution of the problem also with a zero gravity field obtained using the proposed numerical scheme. The dotted curve shows the effect of the gravitational field: both the dotted and dashed curves are exactly of the same profile but one is the translation of the other.

5.4.2. Toro's dam break problem with gravity

For our final experiment we consider the Toro dam break problem with a gravitational source term in the context of gas dynamics. The initial data features an inner constant state $U_{\text{in}} = [1, 0, 2.5]$ for $0.35 \leq x \leq 0.65$ and outer state

$U_{out} = [0.125, 0, 0.025]$ elsewhere on the interval $0 \le x \le 1$ where $U = [\rho, v, p]$. The numerical solution is calculated using the approach presented in Section 3 and the results obtained at time $t_f = 0.125$ are shown in Fig. 14 (red dotted curves) and are compared to the solution of the same problem obtained without the effect of gravitations (blue solid line). Both profiles are identical but shifted due to the effect of gravitation.

6. Conclusion

In this paper we developed a nonuniform extension of the central schemes for the numerical solution of system of conservation laws in one-space dimension to the case of nonuniform grids. The developed method follows the staggered version of the Lax–Friedrichs scheme, and evolves a piecewise linear numerical on a single nonuniform staggered grid. A slopes limiting procedure reduces spurious oscillations. The proposed scheme is then applied and classical gas–solid two-phase flow problems are successfully simulated. A direct comparison between the obtained numerical results and those obtained using Riemann solvers show perfect agreement in all test cases which validate and confirms the efficiency and potential of the proposed method.

We then extended the proposed scheme to the case of the non-homogeneous hyperbolic systems with source terms. In particular, we were interested in the Euler equations for gas dynamics with a gravitational source term. Necessary adaptations of the numerical based scheme were made and classical problems were successfully solved. The effects of the gravitational field are clearly observed in the obtained numerical results where the solution curves are shifted as compared to those obtained in the absence of gravitations. Extensions of the proposed scheme to the case of hyperbolic balance laws are currently being investigated in order to properly treat steady state problems. We are also interested in extending the proposed scheme to higher-order space dimensions.

References

[1] P. Arminjon, D. Stanescu, M.C. Viallon, A two-dimensional finite volume extension of the Lax–Friedrichs and Nessyahu-Tadmor schemes for compressible flows, in: M. Hafez, K. Oshima (Eds.), Proceedings of the 6th International Symposium on Comput. Fluid Dynamics, vol. IV, 1995, pp. 7–14.
[2] P. Arminjon, M.C. Viallon, A. Madrane, A finite volume extension of the Lax-Friedrichs and Nessyahu-Tadmor schemes for conservation laws on unstructured grids, revised version with numerical applications, Int. J. Comput. Fluid Dyn. 9 (1) (1997) 1–22.
[3] B. Cockburn, S.-Y. Lin, C.-W. Shu, Tvb Runge-Kutta local projection discontinuous Galerkin finite element method for conservation laws iii: one dimensional systems, J. Comput. Phys. 84 (1989) 90–113.
[4] V. Deledicque, M.V. Papalexandris, An exact riemann solver for compressible two-phase flow models containing non-conservative products, J. Comput. Phys. 222 (2007) 217–245.
[5] A.I. Delis, T. Katsaounis, Relaxation schemes for the shallow water equations, Int. J. Numer. Methods Fluids 41 (2003) 695–719.
[6] D. Drew, L. Cheng, R.T. Lahey, The analysis of virtual mass effects in two-phase flow, Int. J. Multiphase Flow 5 (1979) 233.
[7] D. Drew, S. Passman, Theory of multicomponent fluids, Appl. Math. Sci. 135 (1998).
[8] H. Enwald, E. Peirano, A.E. Almstedt, Eulerian two-phase flow theory applied to fluidization, Int. J. Multiphase Flow 222 (1986) 21–66.
[9] S.K. Godunov, E. Romenski, Elements of Continuum Mechanics and Conservation Laws, Kluwer Academic/Plenum Publishers, New York, 2003.
[10] A. Harten, B. Engquist, S. Osher, S. Chakravarthy, Uniformly high order essentially non-oscillatory schemes, III, J. Comput. Phys. 71 (1987) 231–303.
[11] M. Ishii, T. Hibiki, Thermo-Fluid Dynamics of Two-Phase Flow, Springer, 2006.
[12] G.-S. Jiang, D. Levy, C.-T. Lin, S. Osher, E. Tadmor, High-resolution non-oscillatory central schemes with non-staggered grids for hyperbolic conservation laws, SIAM J. Numer. Anal. 35 (1998) 2147–2168.
[13] G. Jiang, E. Tadmor, Non-oscillatory central schemes for multidimensional hyperbolic conservation laws, SIAM J. Sci. Comput. 19 (1998) 1892–1917.
[14] P.D. Lax, Weak solutions of nonlinear hyperbolic equation and their numerical computation, Commun. Pure Appl. Math. 7 (1954) 159–193.
[15] S.J. Lee, K.S. Chang, S.J. Kim, Surface tension effect in the two-fluids equations system, Int. J. Heat Mass Transfer 41 (1998) 2821.
[16] R.J. LeVeque, Finite Volume Methods for Hyperbolic Problems, Cambridge University Press, 2002.
[17] R.J. LeVeque, D. Mihalas, E. Dorfi, E. Mueller, Computational methods for astrophysical fluid flow, in: O. Steiner, A. Gautschy (Eds.), 27th Saas-Fee Advanced Course Lecture Notes, Springer-Verlag, 1998.
[18] X.-D. Liu, S. Osher, T. Chan, Weighted essentially non-oscillatory schemes, J. Comput. Phys. 115 (1994) 200–212.
[19] H. Nessyahu, E. Tadmor, Non-oscillatory central differencing for hyperbolic conservation laws, J. Comput. Phys. 87 (2) (1990) 408–463.
[20] J.D. Ramshaw, J.A. Trapp, Characteristics, stability, and short wavelength phenomena in two-phase flow equation systems, Nucl. Sci. Eng. 66 (93) (1978).
[21] A.D. Resnyanskya, N.K. Bourne, Shock-wave compression of a porous material, J. Appl. Phys. 95 (2004) 1760–1769.
[22] E. Romenski, A.D. Resnyansky, E.F. Toro, Conservative hyperbolic formulation for compressible two-phase flow with different phase pressures and temperatures, Quart. Appl. Math. 65 (2007) 259.
[23] L. Sainsaulieu, Finite-volume approximations of two phase-fluid flows based on an approximate Roe-type Riemann solver, J. Comput. Phys. 121 (1995) 1–28.
[24] G.A. Sod, A survey of finite-difference methods for systems of nonlinear conservation laws, J. Comput. Phys. 27 (1978) 1–31.
[25] H. Staedtke, Gasdynamic Aspects of Two-Phase Flow, Wiley, 2006.
[26] H.B. Stewart, Stability of two-phase flow calculation using two-fluid models, J. Comput. Phys. 33 (259) (1979) 259–270.
[27] H.B. Stewart, B. Wendroff, Two-phase flow: models and methods, J. Comput. Phys. 56 (363) (1984) 363–409.
[28] J.H. Stuhmiller, The influence of interfacial pressure forces on the character of two-phase flow model equations, Int. J. Multiphase Flow 3 (551) (1977) 551–560.
[29] E.F. Toro, Shock-Capturing Methods for Free-Surface Shallow Flows, Wiley and Sons Ltd., 2001.
[30] E.F. Toro, Riemann Solvers and Numerical Methods for Fluid Dynamics, 2nd edition, Springer-Verlag, 1999.
[31] R. Touma, Unstaggered central schemes with constrained transport treatment for ideal and shallow water magnetohydrodynamics, Appl. Numer. Math. 60 (7) (2010) 752–766.
[32] R. Touma, P. Arminjon, Central finite volume schemes with constrained transport divergence treatment for three-dimensional ideal MHD, J. Comput. Phys. 212 (2) (2006) 617–636.
[33] R. Touma, Central unstaggered finite volume schemes for hyperbolic systems: applications to unsteady shallow water equations, Appl. Math. Comput. 213 (1) (2009) 47–59.
[34] R. Touma, S. Khankan, Well-balanced unstaggered central schemes for one and two-dimensional shallow water equation systems, Appl. Math. Comput. 218 (10) (2012) 5948–5960.
[35] R. Touma, G. Jannoun, Non-oscillatory central schemes on unstructured grids for two-dimensional hyperbolic conservation laws, Appl. Numer. Math. 62 (8) (2012) 941–955.

[36] I. Toumi, A. Kumbaro, An approximate linearized Riemann solver for a two-fluid model, J. Comput. Phys. 124 (1996) 286.
[37] B. van Leer, Towards the ultimate conservative difference scheme v. a second-order sequel to Godunov's method, J. Comput. Phys. 32 (1979) 101–136.
[38] D. Zeidan, Numerical resolution for a compressible two-phase flow model based on the theory of thermodynamically compatible systems, Appl. Math. Comput. 217 (2011) 5023–5040.
[39] D. Zeidan, R. Touma, On the computations of gas–solid mixture two-phase flow, Adv. Appl. Math. Mech. 6 (2014) 49–74.